Tong *et al. Chin. J. Mech. Eng.* (2020) 33:63
https://doi.org/10.1186/s10033-020-00484-w

Chinese Journal of Mechanical Engineering

ORIGINAL ARTICLE

Open Access

Design of Vegetable Pot Seedling Pick-up Mechanism with Planetary Gear Train

Zhipeng Tong[1,2], Gaohong Yu[1,2*], Xiong Zhao[1,2], Pengfei Liu[1,2] and Bingliang Ye[1,2]

Abstract

It has been challenging to design seedling pick-up mechanism based on given key points and trajectories, because it involves dimensional synthesis and rod length optimization. In this paper, the dimensional synthesis of seedling pick-up mechanism with planetary gear train was studied based on the data of given key points and the trajectory of the endpoint of seedling pick-up mechanism. Given the positions and orientations requirements of the five key points, the study first conducted a dimensional synthesis of the linkage size and center of rotation. The next steps were to select a reasonable solution and optimize the data values based on the ideal seedling trajectory. The link motion was driven by the planetary gear train of the two-stage gear. Four pitch curves of noncircular gears were obtained by calculating and distributing the transmission ratio according to the data. For the pitch curve with two convex points, the tooth profile design method of incomplete noncircular gear was applied. The seedling pick-up mechanism was tested by a virtual prototype and a physical prototype designed with the obtained parameter values. The results were consistent with the theoretical design requirements, confirming that the mechanism meets the expected requirements for picking seedlings up. This paper presents a new design method of vegetable pot seedling pick-up mechanism for an automatic vegetable transplanter.

Keywords: Combined incomplete noncircular gear, Mechanism dimension synthesis, Planetary gear train, Seedling pick-up mechanism

1 Introduction

Seedling transplantation is an important part of vegetable production: over 60% of vegetable varieties adopt a seedling cultivation method [1]. Generally, mechanical transplantation is more efficient and practical than artificial transplantation. The core of an automatic vegetable transplanter are the seedling pick-up mechanism and the seedling planting mechanism. The automatic machine improves the work efficiency and reduces the leakage rate relative to the case of a semiautomatic machine which comprises only a seedling planting mechanism. The seedling pick-up mechanism is the bottleneck in automatic transplanter development.

Robotic seedling pick-up mechanism is widely used and highly practical. It simulates the manual activity of collecting vegetable pot seedlings from a bowl and pushing them into the seedling planting mechanism. Common ways of seedling pick-up are pneumatic mechanism [2], multilink mechanism [3–6], push-out and clamping combined mechanism [7], and their mixed forms. An automatic vegetable transplanter developed by Japan's Yanmar Company [8] combines the gear, linkage, and slipway. In the process of picking up seedlings, the seedling needle is inserted into the bowl, and the bowl-seedling matrix is clamped. The transplanting speed is only 50 plants/min. Using a slipway seedling pick-up mechanism with a pneumatic connecting rod, a study of Yang et al. [9] simultaneously deployed four claws in a row. And they also studied the control system of the whole machine [10, 11]. The mechanism is highly efficient but space consuming. Yu et al. [12–14], Ye et al. [15] and Zhao et al. [16] researched the rotary seedling pick-up mechanism and

*Correspondence: yugh@zstu.edu.cn
[1] Zhejiang Province Key Laboratory of Transplanting Equipment and Technology, Zhejiang Sci-Tech University, Hangzhou 310018, China
Full list of author information is available at the end of the article

then invented and subsequently developed a seedling pick-up mechanism with a series of rotary noncircular planetary gear trains. Their mechanism mainly includes the seedling pick-up arm and planetary gear train driving parts. The seedlings are collected twice per rotation around the circle at a maximum pick-up rate of 90 plants/min.

The abovementioned rotary seedling pick-up mechanisms, whose simplified model is a two-bar series mechanism, can efficiently pick up seedlings and are highly applicable. The seedlings are grasped by the end-effector, which must meet specific motion trajectory requirements. In early research, Yu et al. [13] and Ye et al. [17] designed a novel two-bar mechanism based on the given shape of a gear pitch curve in a planetary gear train and obtained the seedling pick-up trajectory. The trajectory was optimized by adjusting the parameters of the gear pitch curve. Zhao et al. [18] calculated the parameters of a seedling pick-up mechanism by the method of dimensional synthesis based on a given seedling pick-up trajectory. The above methods considered only the trajectory requirements while neglecting the attitude angles of rods at different positions. However, the rod angles (attitude angles of rod) of the mechanism in the stage of seedling pick-up and pushing have a great influence on the success rate of seedling transplantation.

This paper explores the design method of the seedling pick-up mechanism with planetary gear train. The seedling pick-up trajectory and rod angles are considered simultaneously as constraints. Firstly, we studied the relationship between the bar length and bar rotation angle in a two-bar seedling pick-up mechanism. The mechanism was optimized based on the given angle of the seedling pick-up arm and the seedling pick-up trajectory. The mechanism was driven by a planetary gear train for reducing the number of degrees of freedom (DOF). Finally, a virtual prototype was constructed and evaluated in a simulation test using the modeled parameters, and a physical prototype was manufactured. The effectiveness of the scheme was verified by comparing the theoretical and practical trajectories.

2 Motion Trajectory and Rod Angles Modeling of the Seedling Pick-up Mechanism for a Vegetable Transplanter

2.1 Motion Trajectory of the Needle Point and Analysis of the Needle Angle of the Seedling Pick-up Arm

The seedling pick-up mechanism of an automatic transplanter picks up the seedling from the pot and positions it such that, when released, the seedling falls into the planting mechanism to be planted. These actions are then repeated. An analysis of the existing trajectory characteristics of the seedling pick-up mechanism indicated

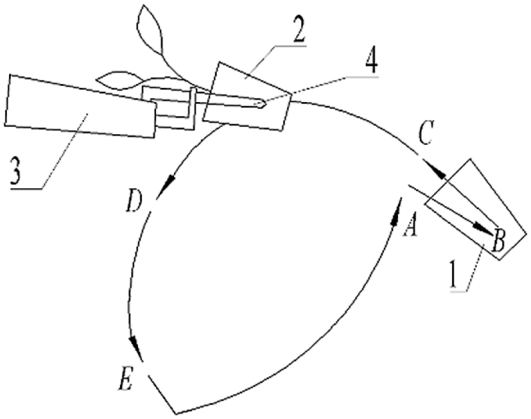

Figure 1 Schematic of the seedling pick-up trajectory: 1. seedling pot, 2. seedling, 3. pick-up arm, and 4. pick-up

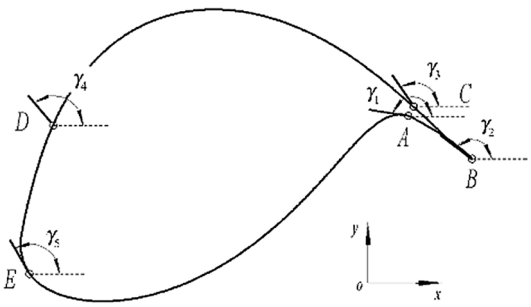

Figure 2 Trajectory and key points for obtaining the required position and orientation characteristics

that the ideal seedling pick-up trajectory requires a sharp beak of a certain length. To meet these requirements, this study proposes the seedling pick-up trajectory drawn in Figure 1. Track *A*–*B*–*C*–*D*–*E* is the point-motion path of seedling pick-up claw 4. During the stage of seedling pick-up (section *A*–*B*–*C*), claw 4 is fully open before dipping into the seedling pot. The claw then clamps the seedling at the bottom of the seedling pot and withdraws it from the pot. During the stage of seedling holding and pushing (section *C*–*D*–*E*), claw 4 moves over the seedling planting mechanism and pushes the seedling into the mechanism. During the stage of return (section *E*–*A*), claw 4 must remain open until next stage of seedling pick-up.

To satisfy the abovementioned pick-up requirements in the context of our previously developed seedling pick-up mechanism [8], this paper describes the seedling pick-up trajectory (Figure 2). The bold line with attitude angle γ in Figure 2 (the orientation of the seedling arm at a certain point) is a simplified trace of pick-up claw 4, and the subscripts of γ denote the key points. Point *A* represents

Table 1 Positions and initial rod angles of the five key points

Key point *i*	1(*A*)	2(*B*)	3(*C*)	4(*D*)	5(*E*)
x_i (mm)	169.47	200.44	171.84	36.20	−23.82
y_i (mm)	18.40	−2.97	22.58	67.78	−64.77
z_i (mm)	171.00	143.00	124.50	130.50	115.00

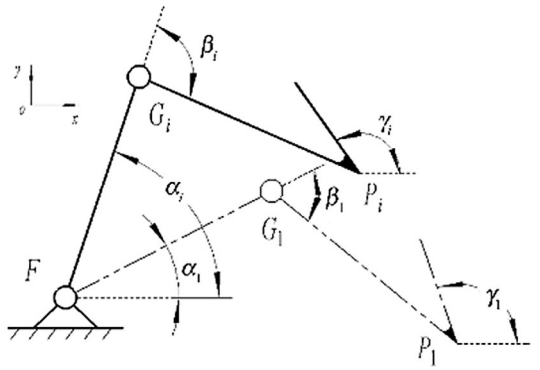

Figure 3 Schematic of the two-bar planar mechanism movement: FG_1 -rod I at key point 1, FG_i - rod I at key point *i*, G_1P_1 - rod II at key point 1, and G_iP_i - rod II at key point *i*

the beginning of the seedling pick-up process. At Point *B*, claw 4 has reached the bottom of the seedling pot. At Point *C*, claw 4 has exited the pot. Point *D* is the location of the seedling holding, and Point *E* represents the finishing point of pushing the seedling into the planting mechanism. The rod angle at Point *E* which affecting the transplanting success rate is the key parameter.

Based on the above analysis of the trajectory and points, the positions and initial rod angles of the five key points (*A*, *B*, *C*, *D*, and *E*) were evaluated and are listed in Table 1.

2.2 Modeling and Analysis of Two-bar Mechanism with Five Key Points

As mentioned in the previous section, the trajectory of the tip point of the claw must meet specific requirements, and the orientation of the pot seedling needs to be adjusted during the movement. Points *A*, *B*, *C*, *D*, and *E* in Figure 1 are the key points of the seedling pick-up trajectory, and the seedling pick-up mechanism should satisfy the requirements of position and orientation.

The working track of the seedling pick-up mechanism is realized via a two-link mechanism. This planar mechanism comprises rod I (*FG*) and rod II (*GP*), and the mechanism moves from point 1 to point *i* (Figure 3). Rod II is the end of the actuator, whose endpoint position (coordinates) and orientation (angle) are known. Denavit and Hartenberg proposed a general method called DH matrix modeling [19], which fixes a coordinate system on each link and describes the spatial relations between two adjacent bars through a homogeneous transformation matrix. In the present study, the transformation relation between different key points is established by their parameter data and the DH matrix; then, the Burmester curve (Eq. (1)) about point G_1 is obtained by four key points, and a univariate higher-degree equation (Eq. (2)) is established by five key points:

$$\begin{aligned} &a_1x_{g1}^3 + a_2y_{g1}^3 + a_1x_{g1}y_{g1}^2 + a_2x_{g1}^2y_{g1} + a_3x_{g1}^2 \\ &+a_4y_{g1}^2 + a_5x_{g1}y_{g1} + a_6x_{g1} + a_7y_{g1} + a_8 = 0, \end{aligned} \tag{1}$$

$$b_1y_{g1}^4 + b_2y_{g1}^3 + b_3y_{g1}^2 + b_4y_{g1} + b_5 = 0, \tag{2}$$

where the variables x_{g1} and y_{g1} are the coordinate values of the hinge point *G* in Figure 3 at the initial position, and the coefficients of the above equations are determined by the elements in the DH matrix, see Refs. [20–25] for details.

Substituting the parameter values in Table 1 into Eq. (2) as derived in the literature mentioned above, one obtains the following equation:

$$\begin{aligned} -0.40515442y_{g1}^4 - 29.068988y_{g1}^3 - 5480.1742y_{g1}^2 \\ +2105570.7y_{g1} + 31999427 = 0. \end{aligned} \tag{3}$$

Solving Eq. (3) and obtaining the real root gives:

$$\begin{cases} y_{g1}(1) = 179.2269, \\ y_{g1}(2) = -15.8986. \end{cases} \tag{4}$$

Substituting the two real solutions into Eq. (1), the real root solution set is obtained:

$$x_{g1}(1) = 200.4036, \tag{5}$$

$$\begin{cases} x_{g1}(2.1) = 23.2990, \\ x_{g1}(2.2) = 165.8176, \\ x_{g1}(2.3) = 454.0944. \end{cases} \tag{6}$$

The qualified solutions are (200.4036, 179.2269), (23.2990, −15.8986), (165.8176, −15.8986), and (454.0944, −15.8986). The above four center and seedling pick-up points share the same coordinate system, as shown in Figure 4.

The line segment G_1P_1 on the simplified model of rod II reaches four possible points (The feasible solution of G_1 in Figure 4). Rod II should not interfere with the seedling pot (Item 1 in Figure 1) or approach it too closely; hence, point 2 (which meets the requirements) is an ideal point.

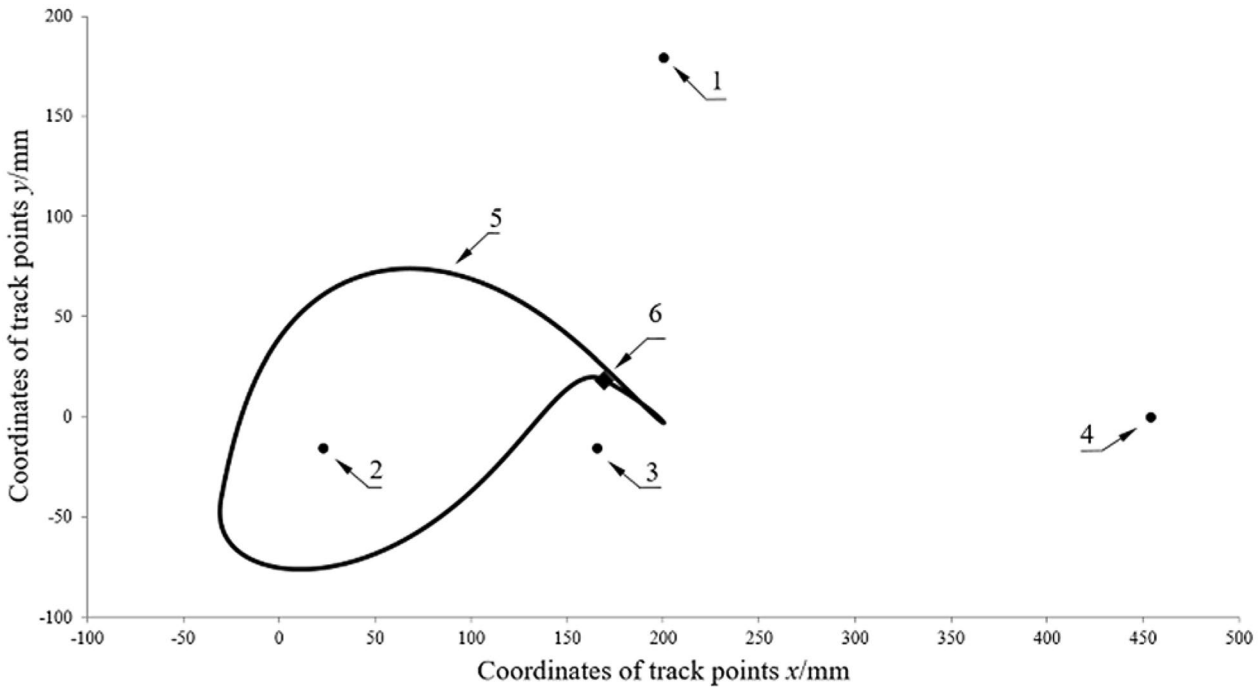

Figure 4 Solution set of the points in the same coordinate system, and plot of the seedling trajectory: 1. Point (200.4036, 179.2269), 2. Point (23.2990, −15.8986), 3. Point (165.8176, −15.8986), 4. Point (454.0944, −15.8986), 5. Seedling pick-up trajectory curve, and 6. End point P_1 of rod II at point 1

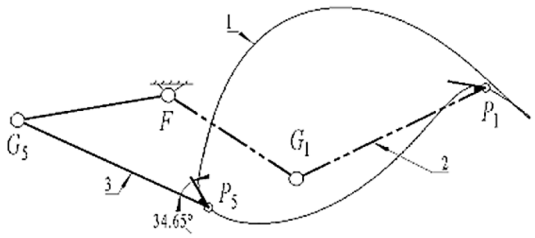

Figure 5 Schematic of the seedling pick-up mechanism calculated from the five key points: 1. Trajectory of seedling pick-up, 2. Key point 1 on rod II, and 3. Key point 5 on rod II

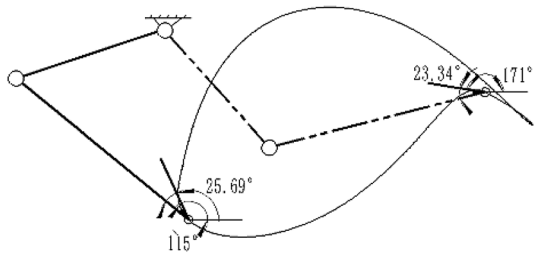

Figure 6 Mechanism before adjusting the rod length parameters

The length of rod II is given:

$$L_{GP} = L_{G_1P_1} = 150.14 \text{ mm}. \tag{7}$$

By solving for the position of F, the solution is obtained:

$$\begin{cases} x_F = x_{F1} = -39.1421, \\ y_F = y_{F1} = 58.6444. \end{cases} \tag{8}$$

The length of rod I is obtained:

$$L_{FG} = L_{FG_1} = 92.24 \text{ mm}. \tag{9}$$

Figure 5 is a schematic of the established seedling pick-up mechanism along with the seedling pick-up trajectory, point 1, and point 5. In this figure, the angle between rod II and the seedling claw (the intersection angle) is 25.74°.

3 Angular Displacement Relationship Model and Single-DOF (SDOF) Model

In the previous section, the relative positional relationships between the key points of the trajectory and the rotating hinge points F of the two bars were preliminarily established through the five key points modeling method, and the lengths of both bars were calculated.

As demonstrated in Figures 2, 5 and 6, the mechanism's movements must meet the trajectory requirements, especially at the closest and farthest track points from the hinge point *F*.

To ensure continuous movements of the connecting rod and to avoid angle mutation caused by an improper length of the two bars (i.e., the bars being too short to reach the farthest point), the state when the endpoint of rod II reaches the farthest point has to be examined. At this point, rods I and II are collinear, and the sum of their lengths is the distance from the farthest point to the hinge point *F*:

$$L_{FG} + L_{GP} = \max(L_{FP_n}) = 247.37 \text{ mm}. \tag{10}$$

Similarly, when the two collinear rods overlap, the endpoint of rod II should be the trajectory point closest to point *F*, which equals the difference between the two lengths:

$$-L_{FG} + L_{GP} = \min(L_{FP_n}) = 43.29 \text{ mm}. \tag{11}$$

By solving Eqs. (10) and (11) as a pair of simultaneous equations, the bar lengths are calculated as follows:

$$\begin{cases} L_{FG} = (\max(L_{FP_n}) - \min(L_{FP_n}))/2 = 102.04 \text{ mm}, \\ L_{GP} = (\max(L_{FP_n}) + \min(L_{FP_n}))/2 = 145.33 \text{ mm}. \end{cases} \tag{12}$$

Figure 7 shows the mechanism after adjusting the bar lengths. A comparison of the bar lengths calculated by using Eqs. (7), (9) and (12) indicates that the angle of the seedling claw satisfies the original five points for both bar lengths; i.e., the angles of point 1 and 5 are 171° and 115°, respectively. At these two positions in Figure 6, the intersection angle is no longer fixed (23.34°≠25.69°). Consequently, the structure of the moving seedling arm changes, which is inconsistent with the actual requirements, so the parameters must be adjusted. To this end, the constraint of the angle is removed, and the intersection angles are unified to 25°. Then, the mechanism is redrawn as shown in Figure 7. In this instance, the seedling pushing angle is 115.69°.

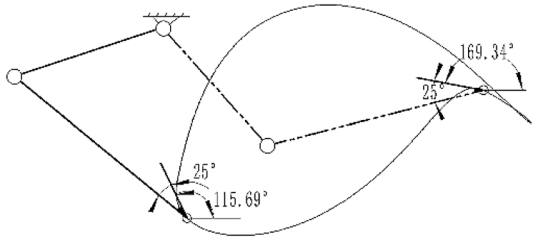

Figure 7 Mechanism after adjusting the rod length parameters

3.1 Angular Displacement Relationship with a 2-DOF Model

Considering the trajectory and posture requirements established above, the motion of rod II is controlled using two servo motors: one at the fixed-hinge point *F* and the other at the moving-hinge point *G* (F_i and G_i, respectively, in Figure 3). The first servo motor (at the fixed-hinge point *F*) is attached to the frame, while the second is attached to rod I.

The first servo motor rotates at constant speed, while the second rotates at a varying speed. The rotation angles of rods I and II at time *t* are $\alpha(t)$ and $\beta(t)$, respectively. The angular displacements of the two bars during one rotation are related as follows.

As shown in Figure 3, rod I rotates by [0, 2π) around the fixed-hinge point *F*, and rod II rotates around the moving hinge point *G* over the range [0, 2π) (relative to rod I). During each rotation, there exist two limit positions: the farthest position superimposed by both bars and the nearest position overlapped by both bars. As shown in Figure 8, the region is divided between the two limit positions. When the endpoint of the seedling claw moves from the farthest to the nearest position of the

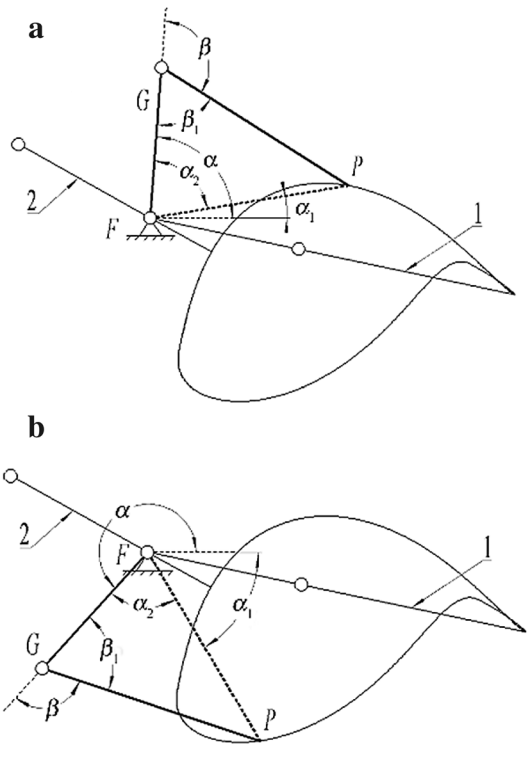

Figure 8 Schematic of the two limit positions of the link motion: **a** the endpoint moves from the farthest to the nearest position of the trajectory; **b** the endpoint moves from the nearest to the farthest position. 1 and 2 indicate the link states in the farthest and nearest limit positions, respectively

trajectory, $\alpha = \alpha_1 + \alpha_2$, and $\beta = \pi - \beta_1$. When the endpoint of the seedling claw moves from the nearest to the farthest position of the trajectory, $\alpha = \alpha_1 - \alpha_2 + 2\pi$, and $\beta = \pi - \beta_1$.

The coordinates (x_f, y_f) of the fixed-hinge point F, the coordinates (x_p, y_p) of the trajectory point P_n, and the lengths L_{FG} and L_{GP} of rods I and II are known. The length from either trajectory point P_n to the fixed-hinge point F is $L_{FP} = \sqrt{(x_p - x_f)^2 + (y_p - y_f)^2}$, and the swing angle is $\alpha_1 = \tan^{-1}((y_p - y_f)/(x_p - x_f))$. The inner angles of the triangle are $\alpha_2 = \cos^{-1}((L_{FG}^2 + L_{FP}^2 - L_{GP}^2)/2L_{FG}L_{FP})$ and $\beta_1 = \cos^{-1}((L_{FG}^2 + L_{GP}^2 - L_{FP}^2)/2L_{FG}L_{GP})$. The calculated rotation angles of rods I and II are location dependent and related through the angular displacement function of the connecting rod:

$$\beta = f(\alpha). \tag{13}$$

By substituting the data values into the angular displacement relationship (Eq. (13)), the angular displacement of rod II relative to rod I is plotted in Figure 9. Note that the initial point of the abscissa is the angular displacement of rod I (−0.2517 rad) when the mechanism moves to the furthest position of the trajectory. At this point, rod I and rod II are collinear and their relative angular displacement is zero.

3.2 2 SDOF Model of the Seedling Pick-up Mechanism

3.2.1 Simplified Model Analysis and Calculation of the Transmission Ratio

To ensure that rod I and rod II in Figure 3 define two hinge point locations of the servo motor, the angular displacement relation shown in Eq. (13) is solved for the rotation angles of the two servo motors.

The transmission of the mechanism is simplified by reducing the input power of the mechanism and transforming the 2-DOF mechanism into an SDOF mechanism. The members must still meet the requirements of Eq. (13) while being suitable for high-speed movement. Two pairs of gear-meshing transmission interactions can transfer the position–speed relationship between the links. The present study adopts a planetary gear train mechanism with a two-stage transmission of four gears (Figure 10). Sun gear 1 and planet gear 4 are fixed to the frame (the ground) and seedling arm 5, respectively. The driving of planet frame 6 moves seedling arm 5. This mechanism has a single DOF.

The angular displacement relationship between the two bars governs the transmission ratio between sun gear 1 and planet gear 4. The total transmission ratio i_z of the two-stage gears is the rotation speed ω_1 of rod I relative to point F divided by the rotation speed ω_2 of rod II relative to rod I:

$$i_Z = \frac{\omega_1}{\omega_2} = \frac{\mathrm{d}\alpha/\mathrm{d}t}{\mathrm{d}\beta/\mathrm{d}t}. \tag{14}$$

The transmission ratio as a function of angular displacement, obtained by substituting the obtained data into the above formula, is plotted in Figure 11, representing a secondary range of the transmission ratio relationship. The starting point of the abscissa is the angular displacement of rod I when the endpoint at point 1.

3.2.2 Distribution of the Total Transmission Ratio

As shown in Figure 10, sun gear 1 meshes with the first middle gear 2, which (along with the second middle gear 3) is fixed to intermediate shaft M. The second middle gear 3 then meshes with planetary gear 4. The meshing motion of sun gear 1 and the first middle gear 2 governs the first transmission ratio, and the meshing motion of

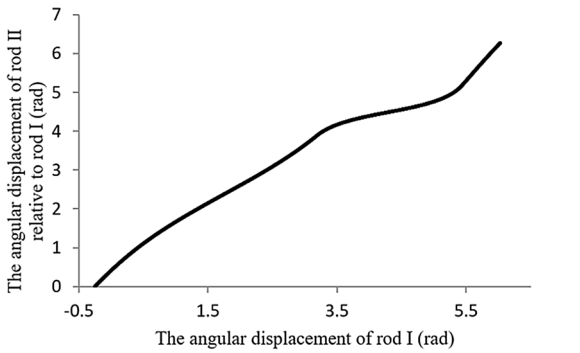

Figure 9 Angular displacement of rod I and rod II

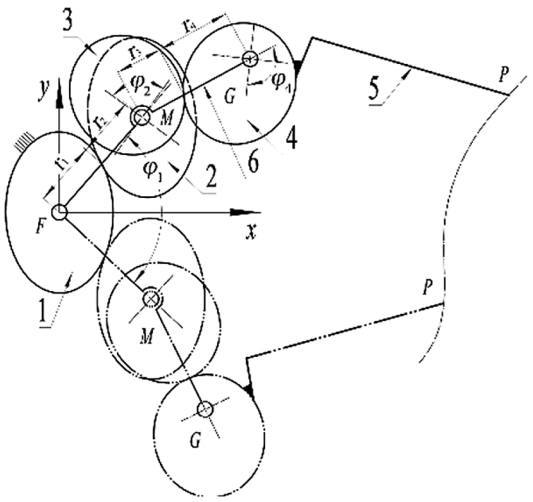

Figure 10 Schematic of the two-stage, four-gear transmission mechanism: 1. Sun gear, 2. First middle gear, 3. Second middle gear, 4. Planet gear, 5. Seedling arm, and 6. Planet frame

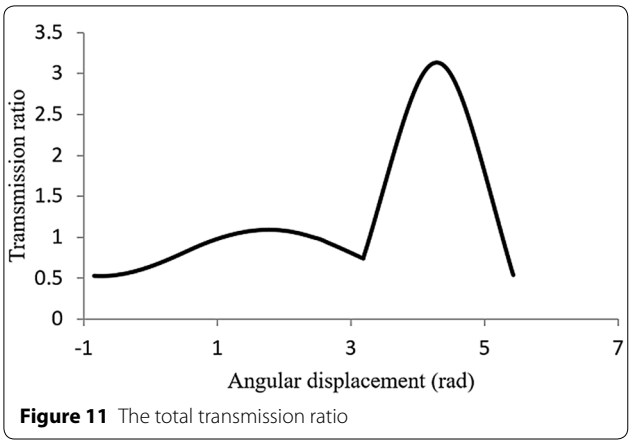

Figure 11 The total transmission ratio

the second middle gear 3 and planet gear 4 governs the second transmission ratio. As the two transmission ratios are independent, their product gives the total transmission ratio. When the total transmission ratio is known, the first transmission ratio can be set, and the second transmission ratio can be solved.

The total transmission ratio in Figure 11 exhibits two unsteady fluctuations, and the second peak is significantly higher than the first. The flatter the transmission ratio curve, the more stable is the curvature radius of the corresponding noncircular gear changes. Therefore, a constant transmission ratio is favorable for generating the tooth profile.

To this end, the first-order transmission was fitted using an elliptic equation. Let r_1 and ϕ_1 be the radius of curvature and angle of rotation of the sun gear, respectively, and let r_2 and ϕ_2 be the corresponding quantities of the first middle gear 2. The elliptic equation of sun gear 1 is given as:

$$r_1 = \frac{a(1-k_1^2)}{1-k_1\cos\varphi_1}, \tag{15}$$

where a denotes the major axis of the ellipse and k_1 is the eccentricity.

The change period of the angle of rotation to diameters r_1 and r_2 is [0, 2π), and the center-to-center distance of the two wheels is a_{12}=2a. Therefore:

$$\begin{cases} r_2 = \frac{a(1-k_1^2)}{1+k_1\cos\varphi_2}, \\ \varphi_2 = 2\arctan\left[\left(\frac{1+k_1}{1-k_1}\right)\tan\frac{\varphi_1}{2}\right], \\ i_{12} = \frac{1-2k_1\cos\varphi_1+k_1^2}{1-k_1^2}. \end{cases} \tag{16}$$

Both peaks in the total transmission ratio curve (Figure 11) should be reduced. The second fluctuation in the total transmission ratio is presumably caused by the transmission of the gear contributing to the transmission ratio i_{12}. The second peak of i_z appears at 245.69°. The transmission ratio i_{12} is a cosine function of the angular displacement (Eq. (16)), which peaks at 180°. Adding the initial phase angle and shifting the abscissa (180°) of the highest point to 245.69°, one obtains:

$$\begin{cases} \varphi_1' = \varphi_1 - 65.69, \\ \varphi_2' = 2\arctan\left[\left(\frac{1+k_1}{1-k_1}\right)\tan\frac{(\varphi_1-65.69)}{2}\right], \\ i_{12}' = -\frac{2k_1}{1-k_1^2}\cos(\varphi_1-65.69)+\frac{1+k_1^2}{1-k_1^2}. \end{cases} \tag{17}$$

The second transmission ratio is:

$$i_{34} = i_z/i_{12}'. \tag{18}$$

The corresponding angle is:

$$\varphi_3 = \varphi_2', \tag{19}$$

$$\varphi_4 = \int_0^{\varphi_3}\frac{1}{i_{34}}\mathrm{d}\varphi_3. \tag{20}$$

Let r_3 and r_4 be the radius of curvature of the second middle gear and planet gear, respectively, and let L be their center distance, given the following conditions:

$$\begin{cases} r_3 + r_4 = L, \\ r_3(\varphi_3) = \frac{L}{1+i_{34}}. \end{cases} \tag{21}$$

When the first transmission ratio curve is selected as the cosine curve, the second transmission ratio curve is the curve with double fluctuation in the cycles. The ratio of the two peaks in the total transmission ratio is approximately 1:3. After the transmission ratios are distributed, the magnitudes of the two peaks in the second transmission ratio curve are nearly equal (ratio 1:1). Under the above constraints, one obtains k_1=0.2702.

By substituting the data into the above equation, the transmission ratios and rotation angles were obtained for all orders. Figure 12 shows three kinds of transmission ratio curves. The angular displacement of the driving gear of the first and total transmission ratios is the rotation angle ϕ_1 of the sun gear, which is uniformly distributed. The angular displacement of the driving gear of the second transmission ratio should equal the rotation angle ϕ_3 of the second middle gear obtained by Eq. (19), which is not evenly distributed.

The red transmission ratio curve in Figure 12 traces the pitch of the elliptic gear, and its pitch curve and tooth profile generation method can be easily identified. The blue transmission ratio curve is a quadratic equal-amplitude transmission ratio curve; Figure 13 shows the corresponding gear pitch curve. As the tooth profile of a nodal curve with two convex points is difficult to generate, the nodal curve was segmented, and two independent

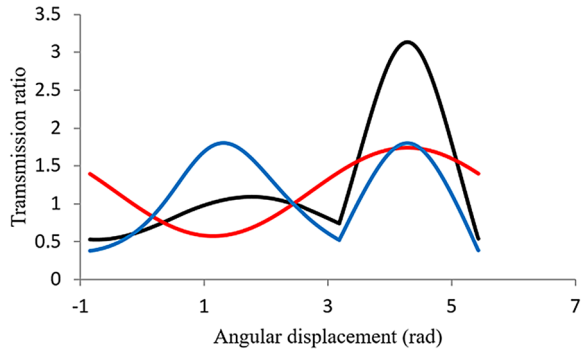

Figure 12 Comparison graphs of three transmission ratios (red line–the first transmission ratio; blue line–the second transmission ratio; black line–the total transmission ratio)

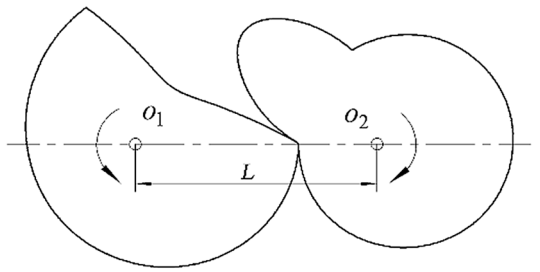

Figure 13 Pitch curve of secondary continuous unequal-amplitude combined gear

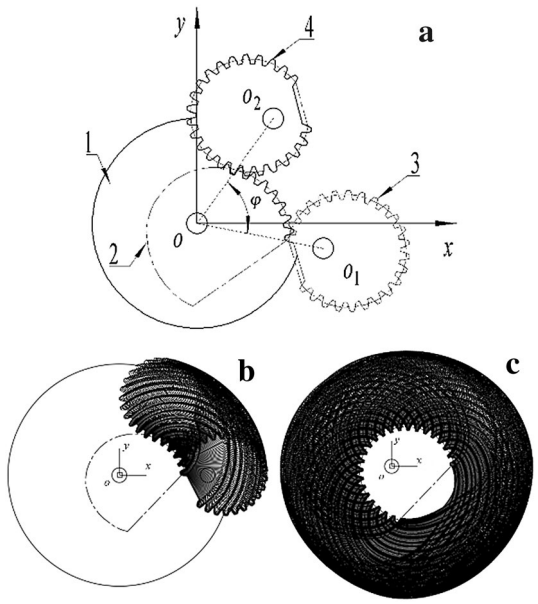

Figure 14 Gear processing method: **a** Schematic diagram: 1. Benchmark gear billet, 2. Processed gear pitch curve, 3. Tool gear in the initial position, 4. Moving tool gear; **b** Process diagram; **c** Finished diagram

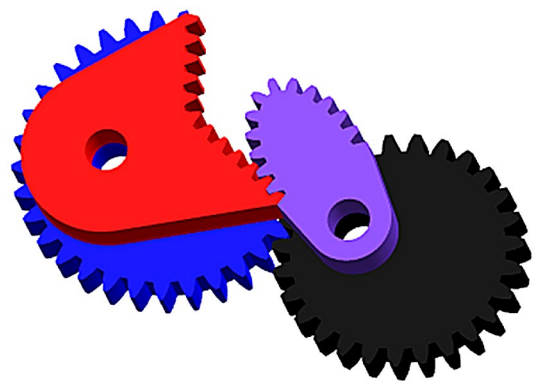

Figure 15 3D model of the quadratic equal-amplitude combined gear

incomplete noncircular gears were fixed in position to form a combined gear. The transmission ratio of the combined gear meets the expected requirements.

The research [26, 27] and processing [28–30] of noncircular gears are quite mature, but there is no corresponding relevant literature on combined gear research. In this paper, a method of noncircular tooth profile generation using simulated gear forming is introduced, which can also be used to design incomplete noncircular gears. In Figure 14, when the tool gear simulates machining noncircular gears, with the benchmark gear billet fixed, the tool gear moves according to the predetermined path, with both gears orbiting around the center of the benchmark gear billet, and rotates around the rotary center of the tool gear itself to ensure that the cutting tool and the tangent to the noncircular gear pitch curve exhibit pure rolling, forming the final tooth profile. A *Visual Basic* control algorithm and the *AutoCAD* Boolean operation enable tooth profile generation. According to the data calculated by Eqs. (15)–(21), the combined gear shown in Figure 15 is constructed.

Considering the strength of the gear, enlarge the center distance of the two-stage gear, set them to 60 mm, and ensure the distance between sun gear and planet gear is 102 mm (Length of rod I in computed result). Double seedling pick-up arms are arranged in the mechanism to improve the effectiveness of transplantation, as shown in Figure 16. The two-clawed seedling pick-up mechanism can pick up seedlings twice when the planet frame rotates once, thereby ensuring high picking efficiency. Two claws are designed rotational symmetrically, and the motion meets the design requirements.

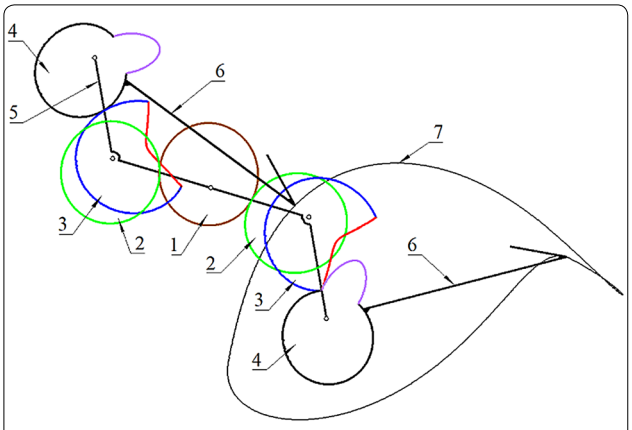

Figure 16 Two-jaw pattern of the seedling pick-up mechanism: 1. Sun gear, 2. First middle gear, 3. Second middle gear, 4. Planet gear, 5. Planet frame, 6. Seedling arm, and 7. Seedling pick-up trajectory

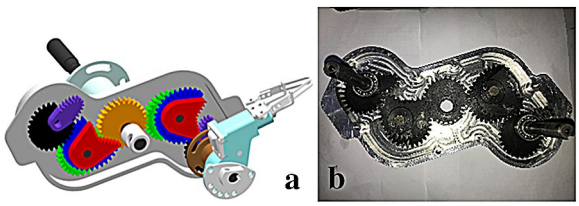

Figure 17 Gears of the planetary gear train: **a** virtual and **b** physical prototype

4 Prototype Test

Based on the node curve optimized in the previous section, virtual and physical gears were constructed (Figure 17). Then, virtual and physical prototypes were designed and manufactured for seedling pick-up. The virtual model was imported into kinematics simulation software to obtain its motion trajectory. The physical prototype was assembled on a test bench for the seedling pick-up test, and a kinematics test with high-speed photography was conducted. The high-speed camera captured the motion trajectory curve in a working period of the seedling pick-up process. The ideal (Figure 2), simulated (Figure 18a) and experimental (Figure 18b) trajectories were compared, and it was found that those trajectories were essentially the same.

Furthermore, as a representative example, the rod angles of the first and fifth key points were tested. The corresponding ideal angles are 169.34° and 115.69°, as shown in Figure 7. The same is true of the value measured

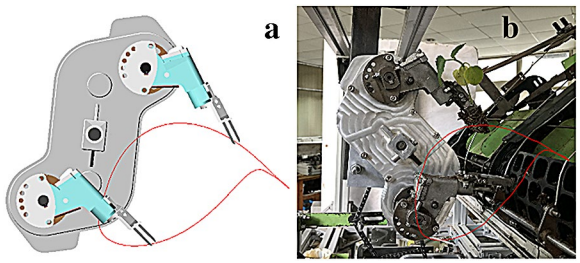

Figure 18 Motion trajectory: **a** virtual and **b** physical prototype

in virtual simulation. In the prototype test, the measured data are 11.20° (supplementary angle of 168.80°) and 65.15° (supplementary angle of 114.85°). There is a slight deviation between the measured data and the ideal value, which is caused by manufacturing and assembly error. Figure 19 shows the angle of the key point 5.

Experiments on seedling pick-up and seedling pushing were carried out with the physical prototype (Figure 20). The results show that the trajectory and the rod angles of the key points meet the expected requirements. The accuracy of the design process and the rationality of the design method are confirmed by validation of the trajectory and key point data. The mechanism designed by this method can efficiently pick up seedlings.

5 Conclusions

The paper proposed a novel seedling pick-up mechanism for an automatic vegetable transplantation machine. The design method of the seedling pick-up mechanism was introduced. The dimensional synthesis of the two-bar mechanism was performed, and the bar lengths and hinge points were calculated via a Burmeister curve model. Under the theoretical and practical constraints, the model data were obtained by appropriate adjustment. The possible mechanism combinations were determined by comprehensively designing the mechanism scales and selecting the structural parameters to obtain superior solutions. The number of DOFs was reduced through a planetary gear transmission mechanism. The mechanism also satisfied the tracking requirements to achieve correct orientation at crucial positions. Furthermore, the method of incomplete noncircular tooth profile generation was also provided. Finally, virtual and physical prototypes of the seedling pick-up mechanism were fabricated to validate the design method. The developed machine can be used to efficiently pick up pot seedlings.

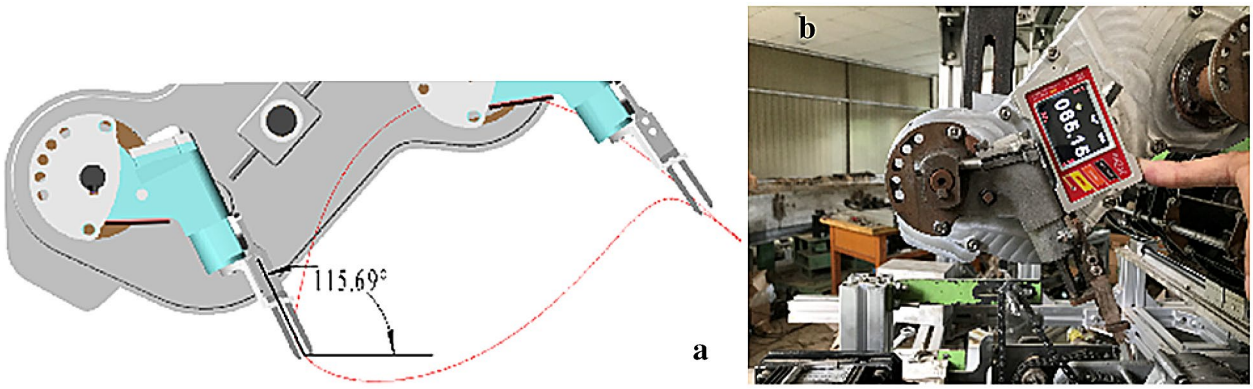

Figure 19 Rod angles at point 5: **a** virtual and **b** physical result

Figure 20 Test of picking up seedlings

Acknowledgements
Not applicable.

Authors' contributions
GY was in charge of the whole trial; ZT conceived the idea and completed most of the research work, then wrote the manuscript; XZ guided the prototype test; PL perfected the formulas and programmed the data; BY gave some advices on the manuscript;. All authors read and approved the final manuscript.

Authors' information
Zhipeng Tong, born in 1992, is currently a PhD candidate at Zhejiang Province Key Laboratory of Transplanting Equipment and Technology, Zhejiang Sci-Tech University, China. He received his bachelor degree from Zhejiang Sci-Tech University, China, in 2014. His research interests include transplanting machinery and agricultural machinery.

Gaohong Yu, born in 1975, is currently a professor at Zhejiang Sci-Tech University, China. He received his PhD degree on agricultural mechanization engineering from Zhejiang University, China, in 2006. His current research focuses on transplanting machines for rice and vegetables.

Xiong Zhao, born in 1982, is currently an associate professor at Zhejiang Sci-Tech University, China. He received his PhD degree from Zhejiang Sci-Tech University, China, in 2014.

Pengfei Liu, born in 1994, is currently a master candidate at Zhejiang Province Key Laboratory of Transplanting Equipment and Technology, Zhejiang Sci-Tech University, China. He received his bachelor degree from Tianjin University of Science & Technology, China, in 2016.

Bingliang Ye, born in 1972, is currently a professor at Zhejiang Sci-Tech University, China. He received his PhD degree from Zhejiang Sci-Tech University, China, in 2013.

Funding
Supported by National Key Research and Development Program of China (Grant No. 2017YFD0700800), National Science Foundation of China (Grant Nos. 51775512, 51575496), and Zhejiang Provincial Natural Science Foundation of China (Grant No. LZ16E050003).

Competing interests
The authors declare no competing financial interests.

Author Details
[1] Zhejiang Province Key Laboratory of Transplanting Equipment and Technology, Zhejiang Sci-Tech University, Hangzhou 310018, China. [2] Faculty of Mechanical Engineering & Automation, Zhejiang Sci-Tech University, Hangzhou 310018, China.

Received: 23 December 2019 Revised: 2 August 2020 Accepted: 24 August 2020
Published online: 10 September 2020

References

[1]. R Tao, X L Cheng, F Q Gao. Analysis on the development and status of dry land transplanting mechanization at home and abroad. *Agricultural Science & Technology and Equipment*, 2016, 3: 40-42. https://doi.org/10.16313/j.cnki.nykjyzb.2016.03.016
[2] Q X Liao, Z Zhang, Q L Hu, et al. Design and trajectory analysis of pneumatic picking-up mechanism for rape paper pot seedling. *Transactions of the Chinese Society for Agricultural Machinery*, 2017, 48(11): 70-78. (in Chinese)
[3] L H Han, H P Mao, F Kumi, et al. Development of a multi-task robotic transplanting workcell for greenhouse seedlings. *Applied Engineering in Agriculture*, 2018, 34(2): 335-342. https://doi.org/10.13031/aea.12462.
[4] L Xin, Z J Lv, W Q Wang, et al. Optimal design and development of a double-crank potted rice seedling transplanting mechanism. *Transactions of the ASABE*, 2017, 60(1): 31-40. https://doi.org/10.13031/trans.11680.

[5] X Jin, D Li, H Ma, et al. Development of single row automatic transplanting device for potted vegetable seedlings. *International Journal of Agricultural and Biological Engineering*, 2018, 11(3): 67-75. https://doi.org/10.25165/j.ijabe.20181103.3969.
[6] M Z Iqbal. Design of a gear driven hopper type dibbling mechanism for a 2.7 kW two-row pepper transplanter. Daejeon: Chungnam National University, 2019. https://doi.org/10.13140/rg.2.2.31847.80807.
[7] E C Armstrong, W A Hanacek, T A Spinetti. Automatic soil plug loader and feeder. US, 4443151, 1984.
[8] K Tsuga. Development of fully automatic vegetable transplanter. *Japan Agricultural Research Quarterly*, 2000, 34(1): 21-28.
[9] Q Z Yang, X Li, X Y Shi, et al. Design of seedlings separation device with reciprocating movement seedling cups and its controlling system of the full-automatic plug seedling transplanter. *Computers and Electronics in Agriculture*, 2018, 147: 131-145. https://doi.org/10.1016/j.compag.2018.02.004.
[10] Q Z Yang, G L Huang, X Y Shi, et al. Design of a control system for a mini-automatic transplanting machine of plug seedling. *Computers and Electronics in Agriculture*, 2020, 169: 105226. https://doi.org/10.1016/j.compag.2020.105226.
[11] Q Z Yang, L Xu, X Y Shi, et al. Design of seedlings separation device with reciprocating movement seedling cups and its controlling system of the full-automatic plug seedling transplanter. *Computers & Electronics in Agriculture*, 2018, 147: 131-145. https://doi.org/10.1016/j.compag.2018.02.004.
[12] G H Yu, B H Liu, Y Zhao, et al. Kinematic principle analysis of transplanting mechanism with planetary elliptic gears in automatic vegetable transplanter. *Transactions of the Chinese Society for Agricultural Machinery*, 2011, 42(4): 53-57. https://doi.org/10.1007/s11460-011-0118-2. (in Chinese)
[13] G H Yu, Z W Chen, Y Zhao, et al. Study on vegetable plug seedling pick-up mechanism of planetary gear train with ellipse gears and incomplete non-circular gear. *Journal of Mechanical Engineering*, 2012, 48(13): 32-39. https://doi.org/10.3901/jme.2012.13.032. (in Chinese)
[14] G H Yu, J P Yu, J H Tong, et al. Design of a conjugate concave-convex non-circular gear mechanism. China Mechanical Engineering, 2016, 27(16): 2155-2159+2165. https://doi.org/10.3969/j.issn.1004-132x.2016.16.005. (in Chinese)
[15] B L Ye, G H Yu, Z W Chen, et al. Kinematics modeling and parameters optimization of seedling pick-up mechanism of planetary gear train with eccentric gear and non-circular gear. *Transactions of the Chinese Society for Agricultural Machinery*, 2011, 27(12): 7-12. https://doi.org/10.3969/j.issn.1002-6819.2011.12.002. (in Chinese)
[16] X Zhao, M Shen, J N Chen, et al. Kinematic analysis and virtual experiment of rotary pick-up mechanism on cotton transplanter. *Transactions of the Chinese Society for Agricultural Machinery*, 2014, 30(8): 13-20. https://doi.org/10.3969/j.issn.1002-6819.2014.08.002. (in Chinese)
[17] B L Ye, X J Jin, G H Yu, et al. Parameter modification guiding optimization design and tests of a rotary transplanting mechanism for rice plug seedlings. *Applied Engineering in Agriculture*, 2015, 31(6): 863-873. https://doi.org/10.13031/aea.31.11198.
[18] X Zhao, J N Chen, Y Wang, et al. Reverse design and analysis of rice seedling transplanter with D-shape static trajectory. *Transactions of the Chinese Society for Agricultural Machinery*, 2012, 28(8): 92-97. https://doi.org/10.3969/j.issn.1002-6819.2012.08.014. (in Chinese)
[19] H Lipkin. A note on Denavit-Hartenberg notation in robotics. In: ASME 2005 International Design Engineering Technical Conferences and Computers and Information in Engineering Conference, Long Beach, California, USA, September 24–28, 2005: 921-926. https://doi.org/10.1115/detc2005-85460.
[20] J Y Han, W X Qian. On the solution of region-based planar four-bar motion generation. *Mechanism and Machine Theory*, 2009, 44(2): 457-465. https://doi.org/10.1016/j.mechmachtheory.2008.03.005.
[21] J Y Han, T Yang. A novel synthesis method for three-position motion generation with planar four-bar mechanisms. In: *ASME 2012 International Design Engineering Technical Conferences and Computers and Information in Engineering Conference*, Chicago, Illinois, USA, August 12, 2012: 419-426. https://doi.org/10.1115/detc2012-70162.
[22] W X Qian, J Y Han. Solution region analysis and robust penalty method of 4-position rigid-body guidance. *Machine Design & Research*, 2008, 24(5): 17-21. https://doi.org/10.13952/j.cnki.jofmdr.2008.06.007. (in Chinese)
[23] E C Kinzel, J P Schmiedeler, G R Pennock. Kinematic synthesis for finitely separated positions using geometric constraint programming. Journal of Mechanical Design, 2006, 128(5): 1070-1079. https://doi.org/10.1115/1.2216735.
[24] T Yang, J Y Han, L R Ying. A unified synthesis method based on solution regions for four finitely separated and mixed "point-order" positions. *Mechanism and Machine Theory*, 2011, 46(11): 1719-1731. https://doi.org/10.1016/j.mechmachtheory.2011.06.008.
[25] C H Chiang, J S Chen. An algebraic treatment of Burmester points by means of three basic poles. *Mechanism and Machine Theory*, 1987, 22(1): 47-53. https://doi.org/10.1016/0094-114x(87)90075-9.
[26] D Mundo. Geometric design of a planetary gear train with non-circular gears. *Mechanism and Machine Theory*, 2006, 41(4): 456-472. https://doi.org/10.1016/j.mechmachtheory.2005.06.003.
[27] F L Litvin, I Gonzalez-Perez, A Fuentes, et al. Design and investigation of gear drives with non-circular gears applied for speed variation and generation of functions. *Computer Methods in Applied Mechanics and Engineering*, 2008, 197(45-48): 3783-3802. https://doi.org/10.1016/j.cma.2008.03.001.
[28] X Lian, Y Y Liu, D Z Li, et al. A linkage model and applications of hobbing non-circular helical gears with axial shift of hob. *Mechanism and Machine Theory*, 2013, 70: 32-44. https://doi.org/10.1016/j.mechmachtheory.2013.07.002.
[29] F Y Zheng, L Hua, X H Han, et al. Linkage model and manufacturing process of shaping non-circular gears. *Mechanism and Machine Theory*, 2016, 96: 192-212. https://doi.org/10.1016/j.mechmachtheory.2015.09.010.
[30] G H Yu, Z P Tong, L Sun, et al. Novel gear transmission mechanism with twice unequal amplitude transmission ratio. *Journal of Mechanical Design*, 2019, 141(9): 092304. https://doi.org/10.1115/1.4043019.